J Appl Electrochem (2013) 43:1101–1116
DOI 10.1007/s10800-013-0626-2

RESEARCH ARTICLE

The role of phosphoric acid in the anodic electrocatalytic layer in high temperature PEM fuel cells

Alin Orfanidi · Maria K. Daletou · Labrini Sygellou · Stylianos G. Neophytides

Received: 11 April 2013 / Accepted: 10 September 2013 / Published online: 1 October 2013

Abstract The poisoning effect and the role of H_3PO_4 (PA) at the anodic electrocatalytic layer of a high temperature polymer electrolyte membrane (HT PEM based on ADVENT TPS®) fuel cell are discussed under the light of cyclic voltammetry, CO stripping, and X-ray photoelectron spectroscopy (XPS) experiments. The catalytic layer was based on both the pyridine-modified multi-wall carbon nanotubes, 30 wt% Pt/(ox.MWCNT)–Py, and on commercial 30 wt% Pt/C, with varying PA loadings on the electrode. At low PA loadings (<3 gPA/gPt), the electrochemically active surface area of Pt decreases significantly under H_2 anode long-term operation, approaching surface Pt utilization <10 %. This degradation is attributed to the formation of pyrophosphoric or triphosphoric acid as well as catalytically H_2 reduced PA species, which block the Pt surface area. As was explicitly detected by means of XPS PA species were displaced from the Pt surface under H_2 or CO exposure. The poisoning effect is reversible as these species can be hydrated back to orthophosphoric acid. The reduced species can be reoxidized into PA at 750 mV versus RHE. On the other hand, the electrochemical interface is stable at PA loadings exceeding 3 gPA/gPt, thus approaching Pt surface utilization >80 % in the long term. This is believed to be a consequence of the more uniform distribution of PA, thus eliminating the PA displacement from the Pt interphase. It is hypothesized that the minimization of the PA poisoning effect at PA > 3 gPA/gPt, may also be a result of more efficient hydration of the catalytic layer that is being achieved through the hydration of the PA in the membrane and in the catalyst layer by the cathodically produced water vapors.

Keywords High temperature PEMFCs · Catalytic layer · Electrochemical interface · Pt utilization · Pt poisoning

1 Introduction

Polymer electrolyte membrane fuel cells, PEMFCs, have attracted a lot of interest since they present constructive simplicity, quick start-up, high efficiency, modularity, and versatility, which make them a promising clean energy technology [1]. The operation of a fuel cell at elevated temperatures allows the exploitation of many system's design and operation advantages. There are a lot of advantages such as the reaction kinetics enhancement, increased CO tolerance of the electrocatalyst, simplification of water and heat management, and the more easily recoverable waste heat, which can be used as an additive energy source in cogeneration systems.

Commercialization of PEMFCs is still significantly restricted by its high content in Pt or other noble metals. This will have significant impact on both the cost of the fuel cell and the quantitative availability of Pt as an abundant raw material for the preparation of the electrocatalytic layers. Reduced cost, resulting from increased catalyst utilization and/or catalyst stability, is highly desirable. The last decade great advances have been made

Electronic supplementary material The online version of this article (doi:10.1007/s10800-013-0626-2) contains supplementary material, which is available to authorized users.

A. Orfanidi · M. K. Daletou · L. Sygellou · S. G. Neophytides (✉)
Foundation of Research and Technology-Hellas, Institute of Chemical Engineering Sciences (FORTH/ICEHT), Stadiou Str., Platani, 26504 Patras, Greece
e-mail: neoph@iceht.forth.gr

toward the optimization and commercialization of HT PEMFCs. Many research studies have focused on the design and optimization of electrocatalytic layers in order to increase the triple-phase boundaries at the electrochemical interface [2–5]. The structure of the catalytic layer usually comprises the catalyst, mainly Pt dispersed onto carbon black and a binder, aiming to the establishment of a 3-D ionic link between the Pt catalyst active sites and the polymer electrolyte. In this way the reaction interface is increased, given that only the Pt particles that are in direct contact with the proton conductor are electrochemically active. In such cases, the uniform mixing of the two components is hard to be guaranteed and part of the electrocatalyst is not used. Moreover, the phosphoric acid presence in the HT PEMFC system creates limitations concerning the slow reaction kinetics of the oxygen reduction reaction, ORR, and reduced oxygen solubility in phosphoric acid. Nevertheless, transport of gases and conductance of electrons and protons to the electrochemical interface must be optimized to provide efficient electrochemical reactions.

In a previous work, a new approach toward the development of Pt-based electrocatalytic layers with increased catalyst utilization for use in high temperature PEMFCs was reported [6]. Surface-modified multi-wall carbon nanotubes, MWCNTs, were used as the support. The aim was to achieve a uniform distribution of polar pyridine groups which can interact with phosphoric acid, on the surface of the carbon support. The polar groups are expected to bind the acid molecules creating proton conductive pathways throughout the catalytic layer resulting in the increase of the three-phase boundary and ultimately the catalyst utilization. Stable and finely distributed Pt catalysts, Pt/(ox.MWCNT)–Py, with nanoparticle size ranging between 2 and 4 nm were obtained.

The high temperature PEM MEAs of this work were based on polymer electrolytes with pyridine containing aromatic polyethers (TPS®) [7–11] provided by ADVENT Technologies SA. Due to the harsh chemical conditions existing in these types of fuel cells, very few polymeric materials can efficiently survive [12]. As reported in the literature, most high temperature (150–200 °C) polymer electrolytes are based on acid–base systems. The structure of ADVENT TPS® consists of polyaromatic backbones that bear polar groups, able to bind strong acids like phosphoric acid. This alternative type of polymeric materials has high thermal, mechanical, and oxidative stability due to the aromatic ether bonds. Additionally, the main or side chain pyridine units strongly bind phosphoric acid, which is retained in the membrane matrix [13]. Doping levels of PA as high as 200 wt% of these polyethers result in membranes with ionic conductivity values as high as 10^{-1} S/cm at 180 °C.

As also mentioned above, the presence of phosphoric acid in the catalyst layer is critical for the creation of an ionic link between the Pt particles and the membrane. The electric fields at electrode/electrolyte interface that is being generated and controlled by the applied potential play a significant role as it does not only affect the double-layer structure influencing the orientation of adsorbed species but also may modify the reactions' pathway and the electrochemical reactions' rate [14]. Phosphoric acid in strong acidic solution (pH lower than 1) is adsorbed on the Pt surface with the non-protonated atom, but becomes ionized as the potential increases. Adsorbed dihydrogen phosphate, $H_2PO_4^-$, presents two coordinations, which are potential depended [15]. Also, PA coverage on Pt increases with potential and the maximum value is obtained at 0.8 V versus NHE, the later was studied in a phosphoric acid solution containing 1 mol/dm^3 $HClO_4$ [16]. It has been reported that phosphoric acid adsorption competes with other molecules like water for the free Pt sites [17, 18]. Anion adsorption, $H_2PO_4^-$ [19, 20] amounts to 4 % of the surface coverage in dilute phosphoric acid at room temperature for an adsorption potential of 0.1 V (RHE). The adsorption of $H_2PO_4^-$ is likely to be appreciably higher in 96 wt% phosphoric acid where the mole ratios of acid and water are shifted to a large excess of $H_2PO_4^-$ anions. Dehydration (or condensation) of orthophosphoric acid leads to its polymerization. In this way, a series of polyphosphoric acids can be obtained. The "backbone" chain of these types of molecules consists of alternating P and O atoms covalently bonded. Polyphosphoric acid molecules can have dozens of such phosphoric units bonded in a row. Phosphoric acid molecules can also be bounded together in rings or from the third –OH group on an orthophosphoric acid unit with other phosphoric groups to form branches in the polyphosphoric/polyphosphate chains.

The hydrogen oxidation is very fast in the HTPEM fuel cells and requires less Pt loading in the electrodes, compared to the cathode electrode. Nevertheless, the available active sites can be significantly reduced due to the adsorption of phosphoric acid species and therefore influence the performance of the anodic electrode [23]. The influence of the operating conditions on the performance of the anodic electrode especially when it operates under reformate conditions motivated us to study the influence of the amount of phosphoric acid in the anodic catalyst layer. In order to understand the performance of the anodic electrode in a high temperature acid-doped PEM fuel cell, the physical chemistry and electrochemistry of PA in the presence of H_2 over the surface of platinum must be understood. As it will be explicitly discussed PA is catalytically reduced on the Pt surface by H_2, thus resulting in the decrease of the electrochemical active surface area. The formation of PA species during normal fuel cell operation

on the Pt surface was evaluated via cyclic voltammetry and CO stripping voltammetry. Also the phosphoric acid species that poison the Pt active sites and the effect of H_2O, CO, and H_2 on the distribution of PA on the Pt surface have been thoroughly investigated by means of XPS. The catalyst layer consisted of the newly synthesized electrocatalyst 30 wt% Pt/(ox.MWCNT)–Py [6], while the commercial 30 wt% Pt/C was also employed for comparison.

2 Experimental

2.1 Materials

Phosphoric acid-doped polymer electrolyte membranes were provided from Advent Technologies S.A. The in-house synthesized 30 wt% Pt/(ox.MWCNT)–Py catalyst used in this study was synthesized according to the literature [6]. Catalyst powder 30 wt% Pt/Vulcan XC-72R was purchased from Tanaka Kikinzoku International. For the construction of the electrodes, carbon cloth supporting layer was purchased from Fuel Cell Earth LLC, Vulcan XC-72R powder from RawChem Ltd and the PTFE dispersion in water from Sigma-Aldrich. For the preparation of Pt unsupported nanoparticles, dihydrogen hexachloroplatinate(IV) hexahydrate 99.95 % (metals basis) and Pt 37.5 % min were purchased from Alfa Aesar and L(+)ascorbic acid 99.0 % from Carlo Erba. 2-Propanol ≤99.8, dimethylacetamide (DMAc), and H_3PO_4 purum p.a. ≥85 % were purchased from Merck or Sigma Aldrich. All chemicals were used as received unless otherwise noted.

2.2 Instrumentation

The electrochemical measurements were performed using a single cell purchased from Fuel Cell Technologies Inc. Both graphite bipolar plates of the single cell had the same single serpentine flow field for the distribution of reacting gases. The active area of the electrodes was 2 × 2 cm. The assembling torque applied for the single cell was 4.8 Nm. The cell was installed in a fuel cell test station which was built in-house and had provisions for controlling temperature, humidification, and flow of reacting gases. The measurements were made in a two-electrode arrangement using an Autolab potentiostat–galvanostat PGSTAT-302. The outlet of the cell's anodic compartment was connected to an OMNISTAR Balzers quadrupole mass spectrometer for the transient and steady state monitoring of the composition of the outlet gas. The size of the Pt nanoparticles of the MWCNT and carbon-based electrocatalysts was characterized by transmission electron microscopy (TEM) on JEOL JEM2100 operating at 200 kV. Equilibrium chemisorption of hydrogen and CO at 40 °C was performed in an automated apparatus (Autosorb-1, Quantachrome) for the determination of the Pt surface H_2 and CO uptake. The Pt particles surface area and dispersion were calculated by assuming a 1:1 H/Pt and CO/Pt atomic stoichiometry.

The photoemission experiments were carried out in a ultrahigh vacuum system equipped with a SPECS LHS-10 hemispherical electron analyzer, which additionally comprises a water-cooled high pressure cell (10^{-3} mbar to 2 bar) connected with the vacuum chambers through a fast entry system, a sample preparation chamber (base pressure 5×10^{-9}) and an analysis chamber with a base pressure $\sim 10^{-10}$ mbar where the XPS measurements took place. The XPS measurements were performed at room temperature using unmonochromatized AlKa radiation under conditions optimized for maximum signal [constant ΔE mode with pass energy of 97 eV giving a full width at half maximum (FWHM) of 1.7 eV for the Au $4f_{7/2}$ peak]. The measurements were recorded at 0° with respect to the sample surface normal. The analyzed area was a rectangle with dimensions 2.5 × 4.5 mm^2.

The sample was mounted on a heated stainless steel holder. The under study electrode was a Pt nanoparticle film interfaced on PA imbibed TPS® membrane. The Pt film was grounded in order to avoid any surface charging during data acquisition.

2.3 Pt film preparation on polymer electrolyte for XPS experiments

2.3.1 Pt thin film fabrication

0.3 ml H_2PtCl_6 (H_2O) 0.25 M was added in 10 ml 3-distilled water. Ascorbic acid (AA) solution was used as reduction agent. 0.07 g AA was diluted in 10 ml 3-distilled water and then mixed with the Pt precursor solution. The solution was then heated at 140 °C on a preheated hot plate for a few minutes until nucleation and crystal growth were observed. The solution prior to heating had a light clear orange color, during the heating process the color changed from light gray to black. As soon as the solution turned black it was removed from the hot plate. The black color of the solution indicates the formation of Pt crystallites. The solution was then left over night at room temperature for ripening. Thereafter, it was poured in an 8-cm diameter glass disk and placed on a hot plate at 140 °C until complete water evaporation. The Pt unsupported nanoparticles formed a thin conductive film. The Pt film was carefully washed several times with 3-distilled water and heated again until complete water evaporation.

The pyridine-based aromatic polyether membrane was immersed in a 85 wt% H_3PO_4 solution at 140 °C for 20 h

in order to obtain the desired phosphoric acid doping level (~200 wt%). The weight gain was calculated by using the sample's weight before and after the immersion. The doped membrane was then pressed against the Pt film for a few minutes, while heating the glass disk on a hot plate at 140 °C. The membrane was carefully lifted from the glass disk surface. The procedure was repeated until desirable conductivity and film thickness were obtained.

2.4 Electrode preparation and MEA assembly

2.4.1 Electrodes' fabrication

The gas diffusion layer, GDL, used in this study was prepared by spraying a slurry made of carbon Vulcan XC-72R and PTFE solution (50 wt% PTFE/C) on carbon cloth, followed by heat treatment at 300 °C under static air for 40 min. The electrodes were prepared using two different optimized methods, depending on the catalyst type. Two types of electrocatalysts were used, Pt supported on carbon black (30 wt% Pt/C) and Pt supported on MWCNTs [30 wt% Pt/(ox.MWCNT)–Py]. The electrodes containing 30 wt% Pt/C were prepared by spraying 2-propanol-Pt/C ink on the GDL. The electrodes were then treated for 12 h at 80 °C and 3 days at 190 °C under vacuum, in order to remove all traces of the organic solvent. The electrodes containing MWCNT-based catalysts were prepared by dispersing the catalyst powder in a 2-propanol/3-D H_2O 2/1 (*v*/*v*) solution. The catalyst slurry was applied on the GDL by a spatula and the electrodes were left over night to dry at room temperature prior heating at 100 °C in an oven for 1 h.

The cathodic electrode's specifications were kept constant for all MEAs. The carbon black-based electrocatalyst (30 wt% Pt/C) was used and the Pt loading was around 2 mgPt/cm^2 in all cases. The electrocatalyst used for the construction of the anodic electrodes differed and the Pt loading varied from 0.20 to 2.15 mgPt/cm^2.

2.4.2 Membrane electrode assembly (MEA)

Before the MEA assembly, a certain amount of phosphoric acid, PA, was sprayed onto the electrodes. The cathodic electrodes were sprayed with 2 gPA/gPt, whereas in the case of the anodic electrodes the ratio of gPA/gPt varied from 0 to 17.8. The electrode active area was 2 × 2 cm. Several MEAs with differences in the anodic electrode were fabricated. The specifications of the anodic electrodes employing either 30 wt% Pt/(ox.MWCNT)–Py (MEAs 1–12) or 30 wt% Pt/C (MEAs 13–15) are depicted in Table 1. In the case of MEAs 1–7 the Pt loading varied, while the amount of phosphoric acid was kept constant per electrode (at 0.0203 gPA/electrode). Whereas for MEAs 9–12 the Pt loading varied, while the amount of phosphoric acid sprayed on the catalyst layer was kept constant, at 2.00 gPA/gPt. Differentiation of the Pt loading in the electrode results in the alteration of the catalyst layer thickness. By keeping the PA per electrode constant, while at the same time varying the Pt loading (ergo catalyst thickness), the PA distribution per volume of catalyst layer will be altered at each case. More specifically, a thin catalyst layer will contain more PA per volume of catalyst layer, as compared to a thicker one, and therefore more PA will be available for the wetting of the Pt particles' surface (gPA/gPt). On the other hand, for the second case, where the gPA/gPt ratio is kept constant, the available PA for the wetting of the Pt particles' surface is expected to be the same for each Pt loading. The second set of MEAs were tested in order to verify that the phenomena that will be described in detail further in this paper are not related to the amount of Pt in the electrode, but are in a direct reliance to the amount of PA present within the catalyst layer. For comparison, a MEA with no PA sprayed at the electrode (MEA 8) was also prepared. The MEAs were fabricated by hot pressing, the phosphoric acid-doped membranes (doping level ~200 wt%) between the two electrodes at 150 °C for 5 min. For comparison reasons, MEAs having similar specifications but employing the commercial 30 wt% Pt/C electrocatalyst at the anodic electrode were also prepared and studied in parallel.

Table 1 Specifications of the MEAs tested and anodic electrodes

Catalyst used	MEA no.	Pt loading (mgPt/cm^2)	PA amount (gPA/gPt)
30 % Pt/(ox.MWCNT)–Py	1	0.20	17.62
	2	0.40	8.81
	3	0.65	5.42
	4	1.02	3.45
	5	1.25	2.82
	6	1.49	2.36
	7	2.06	1.71
	8	2.03	0.00
	9	0.86	2.00
	10	0.29	2.00
	11	0.77	2.00
	12	1.77	2.00
30 % Pt/C	13	1.61	2.00
	14	1.50	2.00
	15	1.64	6.00

Noble metal loading and phosphoric acid, PA, sprayed on the electrodes prior to the MEA assembly

2.5 Electrochemical characterization

2.5.1 Cyclic voltammetry

The pretreatment and investigation of the anodic electrodes, prior to the CO stripping voltammetry measurements, were conducted via linear sweep voltammetry. The potential was cycled between 0.075 and 0.9 V with a scan rate of 10 mV/s. The cell temperature was 140 °C. One compartment was supplied with a constant flow of 200 cc/min of 10 % H_2 in argon and the corresponding electrode acted as the reference electrode. The compartment with the electrode under investigation (working electrode) was fed with 200 cc/min of Ar flow, which was prior humidified by passing through a thermostated humidifier and the partial pressure of water was adjusted at 9.5 kPa by controlling the operating temperature of the humidifier at 45 °C.

2.5.2 CO stripping voltammetry

The electrochemically active surface area, ECSA, of the Pt-based catalyst was determined via CO stripping voltammetry. CO stripping measurements were performed after a standard activation period of 48 h of continuous operation. The cell temperature was kept constant at 140 °C. One compartment was supplied with a constant flow of 200 cc/min of 10 % H_2 in argon and the corresponding electrode acted as the reference electrode. The compartment with the electrode under investigation (working electrode) was fed with 25 % CO in argon (air liquid) at a flow rate of 100 cc/min at open circuit potential. It was found that the maximum coverage with CO was achieved in approximately 8 min. Subsequently, the compartment was flushed with 200 cc/min argon in order to remove all the traces of CO in the gas phase. The argon flow was humidified by passing through a thermostated humidifier kept at a constant temperature of 45 °C, prior to its introduction to the cell. The potential was then cycled between 0.075 and 0.9 V with a scan rate 10 mV/s. To calculate the CO stripping charge, Q_{CO} (in C), the area under the peak that corresponds to the CO electrooxidation was integrated. The second cycle in the same experiment was used for baseline subtraction, considering that during the second cycle CO was absent from the Pt surface. The ECSA in m^2 was determined considering a charge of 420 μC cm^{-2} for CO oxidation that corresponds to a monolayer of adsorbed CO on polycrystalline Pt as follows [21]:

$$\text{ECSA}\ \left(\text{m}^2\right) = Q_{\text{CO}}\,(\text{C})/4.20\ \text{Cm}^{-2}. \quad (1)$$

The CO_2 produced during the CO stripping experiment was recorded at the exit of the working electrode by a quadrupole Mass Spectrometer (Buzzlers Omnistar).

2.6 Treatment of the Pt film surface in XPS chamber

A Pt nanoparticle film deposited on a PA-doped membrane (Sect. 2.3) was exposed to several gas atmospheres for several hours in the high pressure cell chamber of the UHV system. More specifically, the sample was inserted in the high pressure cell and was heated at 200 or 180 °C under H_2, He/H_2O, or CO flows. The He flow was humidified by the use of a water saturator at room temperature (water partial pressure 4 kPa). In the case of He/H_2O exposure, the sample temperature was set at 180 °C for 90 min. The gas flow was adjusted at 100 cc/min by the use of mass flow controller. Each gas exposure of the sample lasted for 4 h. Thereafter, the temperature was lowered to room temperature. As the high pressure chamber was attached on the UHV, the sample was subsequently inserted in the analysis chamber without being exposed to the ambient atmosphere.

After each measurement, the sample was returned to its initial state by a two-step procedure, before its subsequent exposure to another gas atmosphere. Initially, the sample was placed in the high pressure cell under a constant flow of humidified He (100 cc/min) for 90 min at 180 °C. The humidifier was set at room temperature. Subsequently the sample's temperature was lowered to RT and the sample was transferred in the preparation chamber.

2.7 TEM analysis

Post-mortem analysis of the catalytic layer of used membrane electrode assemblies (MEA) was carried out by using transmission electron microscopy (TEM). The electrodes were separated from the membrane after approximately 50 h of continuous fuel cell operation for the evaluation of the Pt particle size distribution and morphology of the electrocatalyst. Adequate amounts of catalysts were scrapped off the used electrodes and were ultrasonically dispersed in water. A drop of the suspension was placed on a 3-mm carbon-coated copper grids (electron microscopy sciences). The Pt particle size distributions were obtained by manually measuring over 800 Pt particles from the TEM pictures. The mean Pt particle size was then calculated using the following equation:

$$D_{\text{APt}} = \Sigma D_{\text{Pt}} N_{\text{D}}/n\ (\text{nm}), \quad (2)$$

where N_D is the number of particles corresponding to a Pt particle size with diameter D_{Pt} (nm) and n is the total number of measured particles. Pt active surface area is calculated by the use of Eq. 3 [6],

$$\text{CSA}_{\text{TEM}} = 6,000/d_{\text{Pt}} D_{\text{APt}}\ \left(\text{m}^2/\text{g}\right), \quad (3)$$

where d_{Pt} is the surface density of bulk Pt (21.4 g/cm^3). Pt utilization (U_{Pt}) can be determined by comparing the results obtained for the ECSA by the CO stripping

Table 2 Mean Pt particle size and active Pt surface area for the 30 wt% Pt/C catalysts, as measured via H_2 chemisorption, CO chemisorption, and TEM imaging

	Pt particle size (nm)	Active Pt surface area (m^2Pt/gPt)
H_2 chemisorption	3.5	80.3
CO chemisorption	3.7	75.8
TEM	3.2	87.6

voltammetry and the Pt surface area (CSA_{TEM}) obtained by post-mortem TEM imaging according to Eq. 4.

$$U_{Pt} = ECSA/CSA_{TEM}. \quad (4)$$

The validity of the method was checked by the determination of the active Pt surface (CSA) by the chemisorption of CO or H_2 on the Pt surface of 30 wt% Pt/C catalyst. Table 2 shows the results obtained from H_2 and CO chemisorption as well as data obtained from TEM imaging for the same catalyst. It is apparent that the results are in good correlation and the maximum deviation between the three methods does not exceed 10 %. Thus CO can be safely used as the probe molecule for the determination of the ECSA by the use of CO stripping voltammetry and can be compared with the Pt surface area determined using TEM post-mortem measurements in order to derive the electrochemically active surface area utilization (U_{Pt}).

3 Results and discussion

MEAs were fabricated employing the 30 wt% Pt/(ox.MWCNT)–Py electrocatalyst at the anodic electrode and the conventional 30 wt% Pt/C at the cathodic electrode. The specifications of the anodic electrodes, Table 1, altered as to differentiate the catalyst layer (CL) thickness and/or the amount of phosphoric acid (PA) sprayed on the electrode. The electrodes were prepared by changing the catalyst loading while keeping constant the sprayed amount of phosphoric acid per electrode or per Pt gram for the MEAs (1–7) and MEAs (9–12) (Table 1), respectively. MEAs employing the commercial 30 wt% Pt/C at the anodic electrodes with similar specifications were also prepared and evaluated.

All MEAs under study require a break-in period of approximately 48 h under the constant low current density of 0.2 A/cm^2 at 180 °C. During this galvanostatic break-in period, the cell performance improves gradually, with the cell voltage to increase by 30–35 mV for the specific current. The voltage increase is attributed to the so called activation of the MEA, although its exact nature has not yet been determined. Plausible reasons causing the improvement in the cell's performance are the decrease of the ionic resistance of the membrane due to humidification and reorganization of the PA/polymer matrix during fuel cell operation, removal of impurities from the Pt active sites, and redistribution of the phosphoric acid in the catalyst layer leading to the increase in the three-phase boundaries. As discussed earlier, only the Pt particles that are in direct contact with the proton conductor are electrochemically active. The phosphoric acid amount in the catalytic layer is a very important and critical parameter for the achievement of a good proton conductive pathway throughout the catalyst layer.

3.1 Determination of the electrochemically active surface area (ECSA)

As has been described in the experimental section, the calculation of ECSA can be determined by the electrochemical oxidation of the pre-adsorbed CO on the Pt electrode. In the case of high temperature PEMFCs, the electrooxidation conditions, i.e., chemisorption temperature and steam partial pressure, can play a significant role on the reliability of the measurements [22]. For the determination of the optimum conditions of CO stripping voltammetry, CO was adsorbed and electrooxidized at various cell temperatures (100–180 °C). As expected the voltage position of the CO electrooxidation peak depends on cell's temperature (Fig. 1a), while the integrated charge under the CO oxidation peaks is constant at temperatures below 140 °C. Thus, it is safe to consider that a full monolayer of adsorbed CO is developed at temperatures below 140 °C. As described in the experimental section, the outlet of the working electrode compartment was monitored by means of a mass spectrometer. It must be noted that there exists a direct correspondence between the calculated area from the CO titration peaks of the CV and the mass spectrometry recorded CO_2 peaks. Figure 2 depicts the ECSA values calculated from the CO uptake measurements (Eq. 1) for electrodes with various Pt loadings (MEAs 1–5, 7, 12), the linear evolution with increasing Pt loading at the electrode confirms the validity of the method for the determination of ECSA. The ECSA was found to be 40 m^2 Pt/gPt, and the post-mortem TEM-derived average Pt particle size was found 6 nm, resulting in $CSA_{TEM} = 46.7$ m^2Pt/gPt. This corresponds to U_{Pt} approximately 90 % for all Pt loadings on the electrode.

3.2 Effect of H_3PO_4 loading on the anode

All MEAs were left under continuous fuel cell operation at 180 °C at 0.2 A/cm^2 under pure H_2/O_2 flows ($\lambda_{H_2} = 1.2$, $\lambda_{O_2} = 2$) for at least 15 h after the break-in period prior to any measurement. Thereafter, cyclic voltammetric experiments

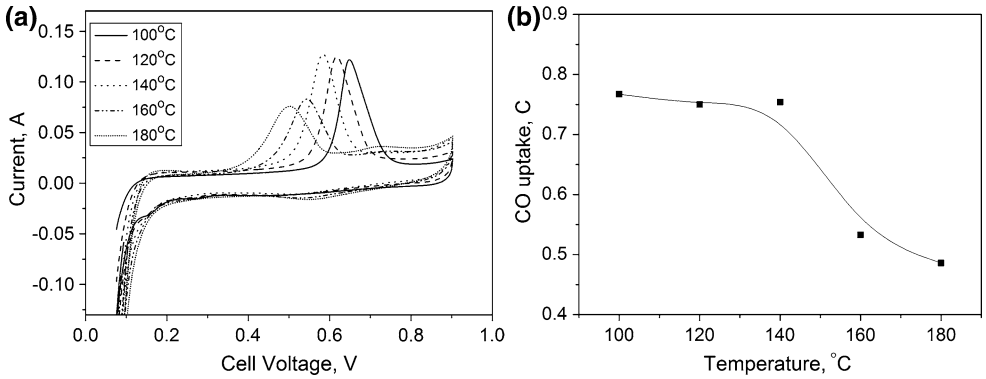

Fig. 1 **a** CO stripping voltammograms at various cell temperatures for constant water partial pressure of 10 kPa and **b** effect of temperature on CO uptake

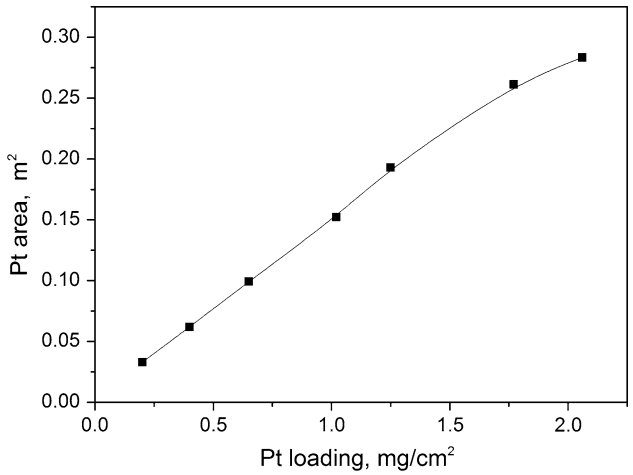

Fig. 2 ECSA determination with increasing Pt loading based on CO stripping voltammetry measurements at 140 °C (MEAs 1–5, 7, 12 in Table 1)

were performed at the anodic electrodes. All cyclic voltammograms were normalized with respect to the Pt loading per electrode for comparison reasons. The first and second recorded cycles for the first set of MEAs 1–7 (Table 1) are presented in Fig. 3a and b, respectively. During the first voltage sweep of the cyclic voltammetry measurements, two oxidation peaks were observed at approximately 500 and 750 mV in the anodic scan. These peaks appear only when the sprayed PA amount on the electrode was below 3 gPA/gPt (Fig. 3a). Interestingly these peaks were not detectable during the second voltage sweep (Fig. 3b). Increasing the gPA/gPt ratio such peaks at 500 and 750 mV do not appear, though a slight increase in the double-layer charging is observed. The above-mentioned behavior and the appearance of the peaks were also observed when electrodes employing the commercial 30 wt% Pt/C were prepared with similar specifications (MEAs 13 and 15) and were used under the same conditions(see supporting information, Fig. S1). In order to clarify whether the aforementioned oxidation peaks are related to the amount of Pt and/or the double-layer charging, a set of MEAs was tested, where Pt loading was varied from 0.29 to 1.77 mgPt/cm^2 and the ratio of gPA/gPt was kept at constant 2 gPa/gPt for all cases (MEAs 10–12). The first and second recorded cycles are present in Fig. 4. It is clear that the appearance of the two oxidation peaks at 500 and 750 mV is not related to the Pt loading but instead to PA amount sprayed in the electrodes, which is within the region that the above observed anodic peaks appear. Also it has to be noted that when similar experiments were conducted at the cathodic electrode for low PA amounts in the electrodes, no such peaks were observed thus showing that the appearance of these peaks is directly related to the anodic process.

Similar peaks were reported by Buelte et al. [23] in a half cell apparatus using standard Pt/C-based electrode, especially at high phosphoric acid concentration, 115 wt% phosphoric acid (75 wt% P_2O_5). They assumed that those peaks during CV are the result of phosphoric acid species adsorption on the Pt surface and subsequent oxidation followed by polarization [23]. Several studies in the literature report the appearance of a peak at around 0.7 V when performing cyclic voltammetry of Pt in different phosphoric acid-based systems [18, 24–29]. The peak was attributed to the anodic oxidation of impurities formed electrochemically from the phosphoric acid in the hydrogen region; phosphine formation by direct reduction of H_3PO_4 or by a partial disproportionation of phosphorous with simultaneous formation of oxyacids such as H_3PO_3, adsorbed at low potentials.

However, Burke and Morrissey [30] gave another explanation for the peak's origin and concluded that it arises from the pre-monolayer oxidation processes and is independent of the electrolyte anion, therefore it is a property of the metal rather than the electrolyte. This hypothesis was supported by the observation of a similar peak in systems not involving phosphoric acid [31, 32]. The reaction producing the peak under low water environments (dehydrated) was reported to be slow [32] and was described as the formation of submonolayer quantities of hydrous oxide films where the reduced state is a Pt adatom, rather than a normal surface or bulk lattice atoms [31].

The cumulative built-up of the species that appear in the CVs of Figs. 3 and 4 at 500–750 mV is shown in Fig. 5 for

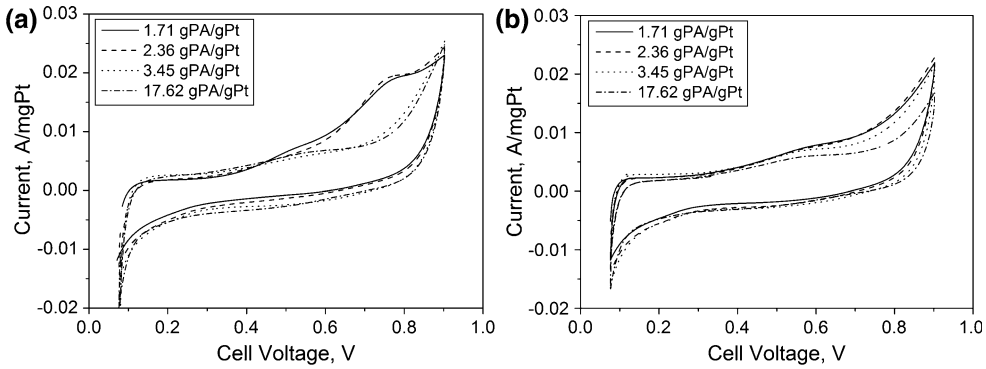

Fig. 3 Cyclic voltammograms **a** first cycle and **b** second cycle at 140 °C after fuel cell operation at 180 °C for 24 h at 0.2 A/cm^2 under pure H_2/O_2 flows ($\lambda_{H_2} = 1.2$, $\lambda_{O_2} = 2$) for MEAs 1, 4, 6, and 7. Variation of the Pt loading with constant amount of PA on the catalytic layer

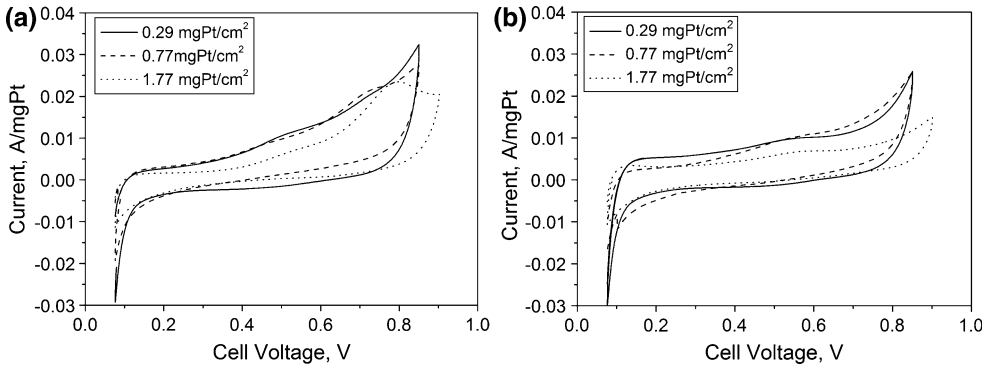

Fig. 4 Cyclic voltammograms, first (**a**) and second (**b**) cycle, at 140 °C after fuel cell operation at 180 °C for 24 h at 0.2 A/cm^2 under pure H_2/O_2 flows ($\lambda_{H_2} = 1.2$, $\lambda_{O_2} = 2$) for MEAs 10–12, where the Pt loading per electrode varied and gPA/gPt = 2

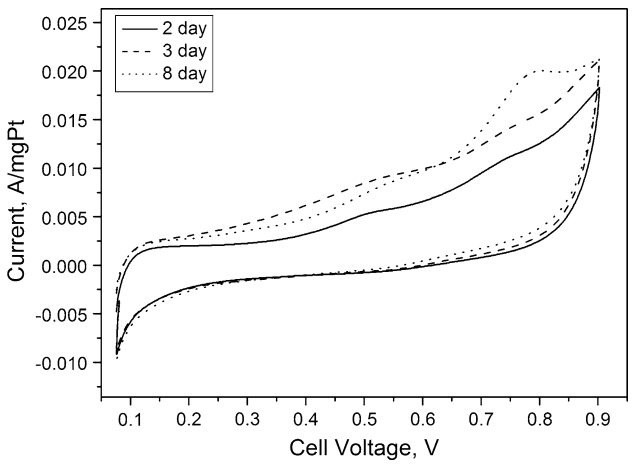

Fig. 5 Cyclic voltammograms (first cycle) of MEA 13 employing the commercial 30 wt% Pt/C catalyst at 140 °C after continuous fuel cell operation at 180 °C at 0.2 A/cm^2 under pure H_2/O_2 flows ($\lambda_{H_2} = 1.2$, $\lambda_{O_2} = 2$) for 2, 3 and 8 days

different MEAs left under constant polarization mode at 0.2 A/cm^2 for longer operation intervals. As depicted in Fig. 5, the CVs were obtained after 2, 3, and 8 days of continuous fuel cell operation at 180 °C. The increase of the intensity of the peaks with time is apparent and denotes the accumulation of electroactive species on the Pt surface. For the anodic electrodes with PA loading higher than 3 gPA/gPt, no peaks were noticed during the first CV cycle with respect to the operation time. On the other hand, for PA loadings lower than 3 gPA/gPt, an increased variation of the peak intensity at 750 mV on the duration of the cell's operation was observed in all cases.

During all the above voltage sweeps, the outlet of the working electrode compartment was monitored using an on-line mass spectrometer. In the course of the potentiodynamic scan of the electrode, production of CO_2 was recorded. As depicted in Fig. 6, the CO_2 MS signal is plotted versus potential. The observed CO_2 production is a result of the carbon substrate's electrooxidation during cyclic voltammetry and is not correlated with the anodic peak at 750 mV. Interestingly, the intensity of the CO_2 formation followed a very specific pattern when relatively low amounts of PA (below 3 gPA/gPt) were present in the catalyst layer. A striking difference between the first and second cycle of the cyclic voltammograms is the increase in CO_2 electrooxidation rate during the second cycle. This is accompanied by the non-appearance of the oxidation peak at 750 mV. The low CO_2 electrooxidation rate observed during the first cycle in Fig. 6 is indicating either a blockage of the electrochemically active surface area or a reconstruction of the electrochemical interface. The hysteresis observed in the CO_2 signal during the first cycle can be attributed to the activation of the electrochemical surface after the appearance of the oxidation peak at 750 mV. Further potential cycling after the second cycle did not result in any additional change either in the voltammogram or the amount of CO_2 production. A totally different

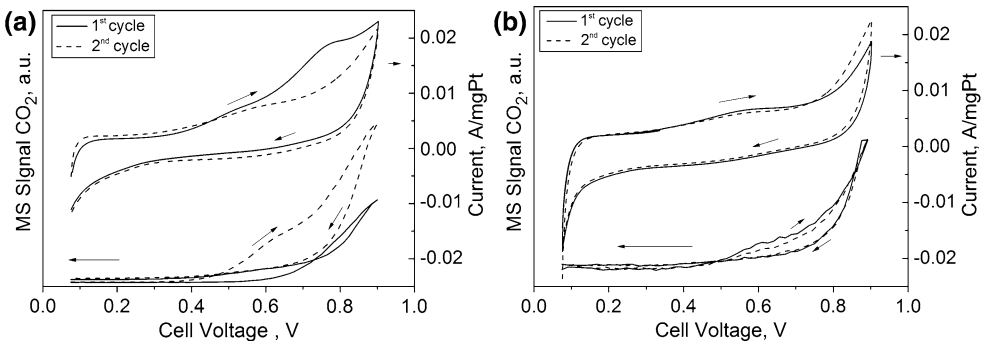

Fig. 6 Cyclic voltammograms (first and second cycle) at 140 °C and the corresponding CO_2 signal as recorded from the on-line mass spectrometer at the outlet of the working electrode's compartment of **a** MEA 7 (1.71 gPA/gPt) and **b** MEA 1 (17.62 gPA/gPt), after fuel cell operation at 180 °C for 24 h at 0.2 A/cm^2 under pure H_2/O_2 flows ($\lambda_{H_2} = 1.2$, $\lambda_{O_2} = 2$)

behavior is observed in the case of high gPA/gPt > 3. As it is depicted in Fig. 6b, there is no difference between the first and second cycle either in the CV or the CO_2 signal.

Polarization curves were obtained from various MEAs with different anodic electrode specifications for the evaluation of the effect depicted in Fig. 6 on the performance of the MEAs after short-term operation. Figure 7 depicts three characteristic IV plots where the PA amount differs in the catalytic layer of the anodic electrode, while maintaining the cathodes specification constant for all cases. Each diagram shows two IV curves. The first was recorded after the continuous fuel cell operation of the MEA for 48 h at 0.2 A/cm^2 under pure H_2/O_2 flows ($\lambda_{H_2} = 1.2$, $\lambda_{O_2} = 2$). Subsequently a CV was carried out within the potential range of 0.075–0.9 V and the polarization curve of the same MEA was recorded again. The electrode with 5.42 gPA/gPt, i.e., higher than 3 gPA/gPt, did not exhibit any apparent changes in the performance (Fig. 7a). An improvement in the performance especially at high current densities is observed for the low gPA/gPt ratios after the CVs were carried out (Fig. 7b, c). The improvement is more significant or otherwise the long-term degradation is larger upon decreasing the gPA/gPt ratio. Although the MEAs had different Pt loadings, the highest performance is observed for the MEA with the lower Pt loading (0.65 mg/cm^2) and the highest ratio of gPA/gPt, while the lowest performance is observed for the anode with the highest Pt loading (2 mg/cm^2) without PA sprayed on the anode. It must be noted that in the later case the electrochemical interface must be formed by the diffusion of part of PA from the membrane. These results indicate two issues regarding the effect of the amount of PA on the electrode:

(1) Increased amount of PA at the anode is beneficial for the efficient performance of the anode and more importantly with significantly lower degradation.
(2) Decreased amount of PA affects both the performances and induces higher degradation rate due to the formation of reduced species on the electroactive Pt surface.

The long-term poisoning effect of the lower quantities of the PA on the electrode is observed at high current densities where the turnover of the electrochemical interface is higher.

In order to confirm that the cell performance improvement upon potential cycling is due to the "re-activation" of the Pt active sites, the ECSA of the different MEAs was measured after several hours of continuous fuel cell operation by means of CO stripping voltammetry. After the first CO stripping measurement, a second CO stripping experiment was sequentially carried out. The outlet gas of the working electrode was monitored with an on-line mass spectrometer. At high gPA/gPt > 3 ratio on the electrode, the measured CO uptake and consequently the calculated ECSA in the first and second CO stripping experiments were exactly the same. On the other hand, for the MEAs with low PA loading in the anodic CL (<3 gPA/gPt), the CO stripping experiment gave very different results before and after the CV. Figure 8 shows an example for MEA 9. In this figure, the two subsequent CO stripping measurements are depicted, along with the corresponding MS signal of CO_2 at the electrode's outlet, produced during CO electrooxidation. As can be seen in Fig. 8a (first CO stripping), immediately after 15 h of continuous fuel cell operation at 0.2 A/cm^2, the measured CO oxidation peak was very small, which is also confirmed by the MS CO_2 signals. As expected in the second sequential CO adsorption and stripping voltammetry (Fig. 8b), the CO electrooxidation peak in the CV and the MS CO_2 signal are 11 times larger than the initial measurement (Fig. 8a). Therefore, it becomes obvious that at low PA loadings and after a certain time of operation the real ECSA decreases. It can be recovered after the CVs depicted in Figs. 3, 4, 5, 6 and the oxidation of the electroactive species at 750 mV. This phenomenon can have a negative influence in the long-term performance of the anodic electrode.

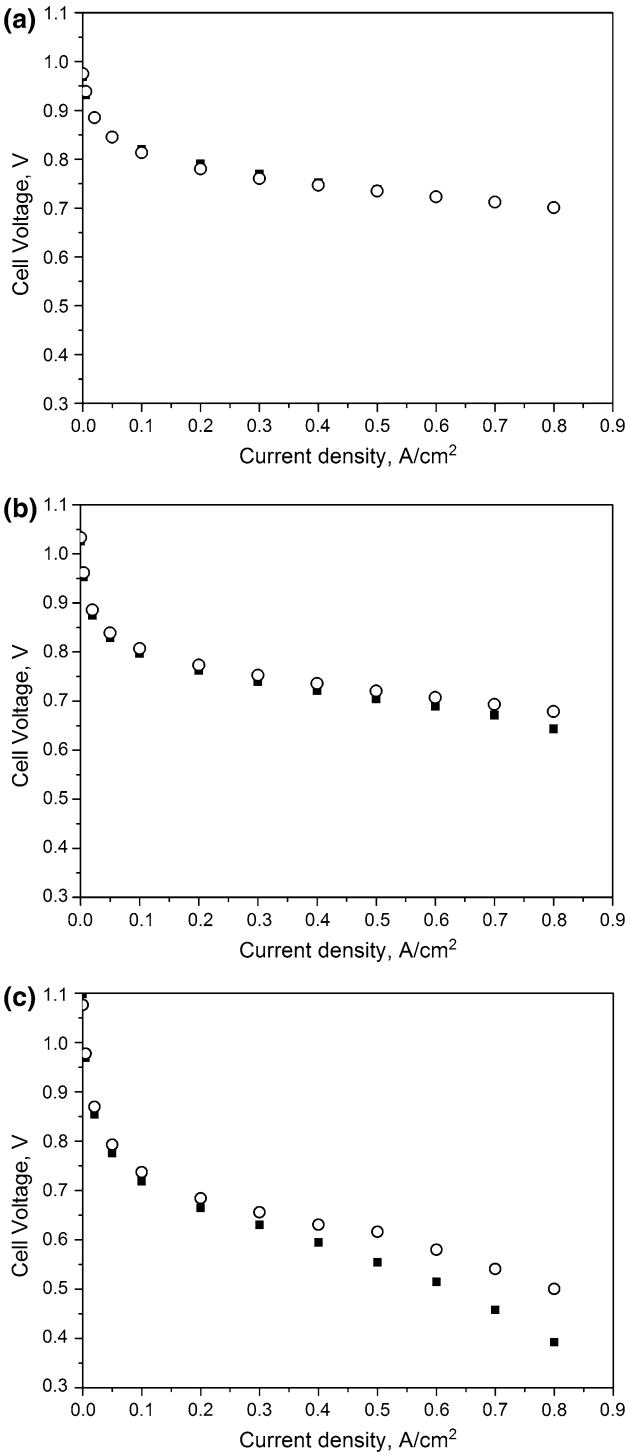

Fig. 7 Polarization curves, IR drop corrected, after the break-in period (24 h in operation at 0.2 A/cm^2) at 180 °C before and after the cyclic voltammogram measurements for MEAs with different amount of sprayed PA at the anodic electrode under H_2 and O_2 flows (200 cc/min, respectively): **a** MEA 3 (5.42 gPA/gPt), **b** MEA 12 (2.00 gPA/gPt), and **c** MEA 8 (0 gPA/gPt). *Black squares* before the CV and *open circles* after the CV

Based on the results of Fig. 8, it can be concluded that under low PA loading on the anodic electrode only <10 % of the Pt active surface is electrochemically active under fuel cell operating conditions. However, the image is drastically different at high gPA/gPt > 3 loadings from that depicted in Fig. 8. The initial CO adsorption coverage is not inhibited but instead is identical to the subsequent adsorption and CO stripping experiment, thus implying a stable and high Pt surface utilization (>80 %), as the ECSA was found to be approximately 39 m^{2}Pt/gPt. In this respect similar long-term performance can be achieved at very low Pt loadings (0.2 mg/cm^2) by adjusting the gPA/gPt ratio at the anode. This is clearly shown in Fig. 9 where the performance of MEA 1 and MEA 7 after the break-in period is almost identical though the Pt loading at the corresponding anodes differs by a factor of 10. This can be attributed to the fact that in the case of MEA 7 the low PA loading may result in a tenfold decrease in the ECSA according to the findings of Fig. 8. On the contrary, almost full exploitation is achieved in MEA 1 which has 10 times lower Pt loading due to its high gPA/gPt ratio.

In order to shed more light in these phenomena, CO stripping experiments were carried out after the electrode exposure in dry and humidified H_2 and Ar atmospheres for 24 h at open circuit potential, where the cell's temperature was set at 180 °C. As depicted in Fig. 10, a fourfold inhibition of CO oxidation peak is observed when the Pt electrode is exposed under dry Ar compared to the exposure of the same electrode under Ar/H_2O flow. This can be rationalized by considering that under dry Ar flow the formation of pyrophosphoric or triphosphoric acid is formed that blocks the Pt surface. This type of fuel cells usually operates at a temperature range of 160–180 °C. As has been mentioned in the introduction, within this temperature range phosphoric acid is known to dehydrate and polymerize, creating polyphosphoric acid species. When two molecules of orthophosphoric acid are dehydrated, they create pyrophosphoric acid releasing a water molecule. A general formula for such poly-acid compounds is $HO(PO_2OH)_xH$, where x is the number of phosphoric units in the molecule. Buelte et al. [23] reported that prolonged exposure of a Pt electrode in phosphoric acid using a half cell set up, resulted in the decrease of the electrocatalyst active area. The later was enhanced as the phosphoric acid concentration increased from 105 to 115 wt% phosphoric acid solution and it was attributed to the formation of polyphosphates on the Pt surface.

In both H_2 flow conditions (i.e., dry or humidified), the CO stripping spectra show significant decrease in the CO oxidation peak. Thus beyond the formation of polymeric dehydrated forms of PA that can be adsorbed strongly on Pt, other specific interactions of H_2 with PA can be the

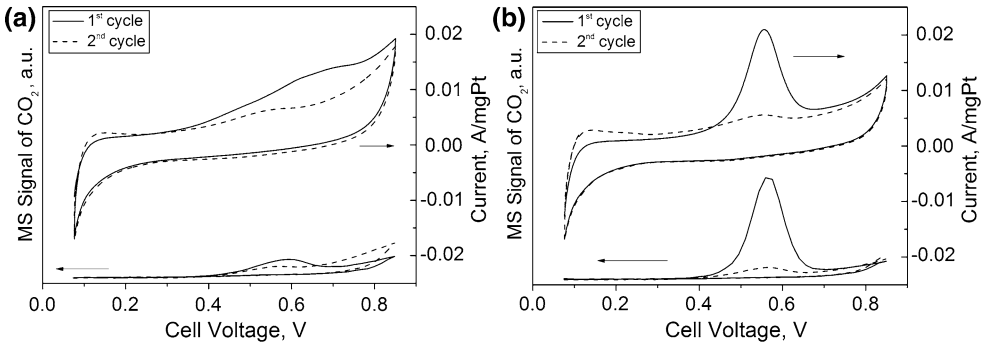

Fig. 8 Voltammograms of adsorbed CO electrooxidation (first and second cycle) at 140 °C and the corresponding CO_2 signal as recorded from the on-line mass spectrometer at the outlet of the working electrode's compartment, **a** before CV and **b** after CV for the anodic electrode of MEA 9 after fuel cell operation at 180 °C for 24 h at 0.2 A/cm^2 under pure H_2/O_2 flows ($\lambda_{H_2} = 1.2$, $\lambda_{O_2} = 2$)

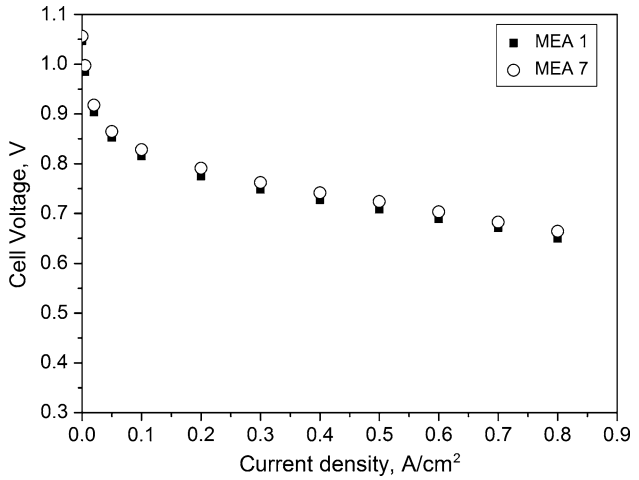

Fig. 9 Polarization curves recorded after 24 h of operation at 0.2 A/cm^2, IR drop corrected, at 180 °C for MEAs with different Pt loading and amount of sprayed PA at the anodic electrode under H_2 and O_2 flows (200 cc/min, respectively). MEA 1:0.2 mgPt/cm^2 and 17.62 gPA/gPt and MEA 7:2.06 mgPt/cm^2 and 1.71 gPA/gPt

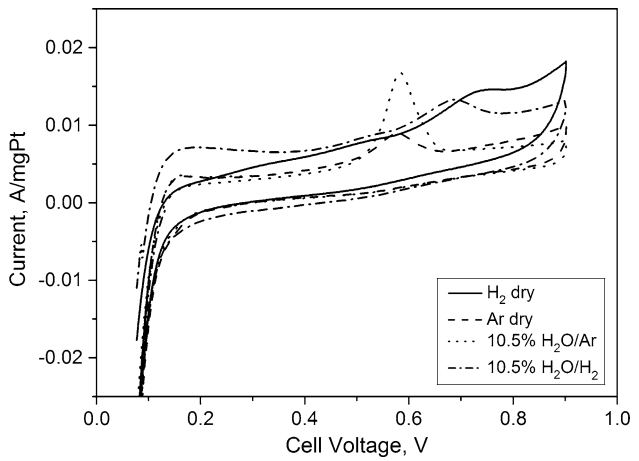

Fig. 10 CO stripping experiments at 140 °C of MEA 14 employing 30 wt% Pt/C. Before each measurement, the working electrode was pre-exposed at OCP and 180 °C for 18 h under dry H_2, dry Ar, 10.5 kPa H_2O/Ar, and 10.5 kPa H_2O/H_2 flows, while the counter electrode was fed with Ar/H_2O

reason for the significant decrease of either the Pt CO uptake or the decrease of the CO oxidation peak. This can be chemical reduction of PA and formation of reduced species or even displacement of PA from catalyst surface, thus inducing shrinkage of the electrochemical interface.

3.3 XPS measurements of the Pt/PA interface

Taking into consideration all the aforementioned information, the reversible degradation observed at low PA loadings on the anodic electrode can possibly be a complex phenomenon that can be attributed either to oxidizable species, which is formed during fuel cell operation and its exposure to H_2, thus blocking the Pt surface, or due to restructuring of the electrochemical interface because of the displacement of the PA from the catalytic layer.

The clarification of the aforementioned processes was attempted by means of XPS. A Pt film deposited on a PA-doped membrane was exposed to several gas atmospheres for several hours in the atmospheric pressure chamber of the ultrahigh vacuum system equipped with XPS (see experimental). The BE values for the main detectable elemental states were obtained from the spectra of the O1s, Pt4f, and P2p regions (Table 3; Figs. 11, 12). The binding energy of Pt4f spectra is shown in Fig. 11a, where the doublet with binding energies 71.4 (Pt $4f_{7/2}$) and 74.7 eV (Pt $4f_{5/2}$) is attributed to metallic Pt for all measurements [33]. It is obvious that the different experimental conditions did not affect the binding energy or the oxidative state of Pt. The later confirms the validity of our measurements since no charging of the surface occurred during measurements.

The various recorded spectra of P2p are shown in Fig. 11b. As also shown in Table 3, there is an apparent shift in the binding energies of the P2p peaks, which depend on the temperature and gas phase pretreatment of the sample. The peak at 133.9 eV of spectrum 2 in Fig. 11b, is attributed to ortho-phosphate ($H_2PO_4^-$) species

Table 3 XPS binding energies with the corresponding FWHM in the braquets, intensity ratio of O1s of (peak II)/(peak I), as well as the atomic ratio *O*/*P*

Experimental conditions	BE (FWHM) (eV) P2p	BE (FWHM) (eV) O1s	O1s intensity ratio (peak II)/(peak I)	*O*/*P* atomic ratio
200 °C 4 h H_2 (1)	134.8, 131.0 (3.2)	532.0, 533.5 (2.4)	1.44	2.48
180 °C 1.5 h H_2O/He (2)	133.9 (3.0)	531.9, 533.3 (2.7)	0.57	3.60
200 °C 4 h UHV (3)	134.8 (3.0)	531.7, 533.4 (2.7)	1.28	3.18
200 °C 4 h CO (4)	134.8 (3.0)	532.0, 533.5 (2.4)	1.34	3.32

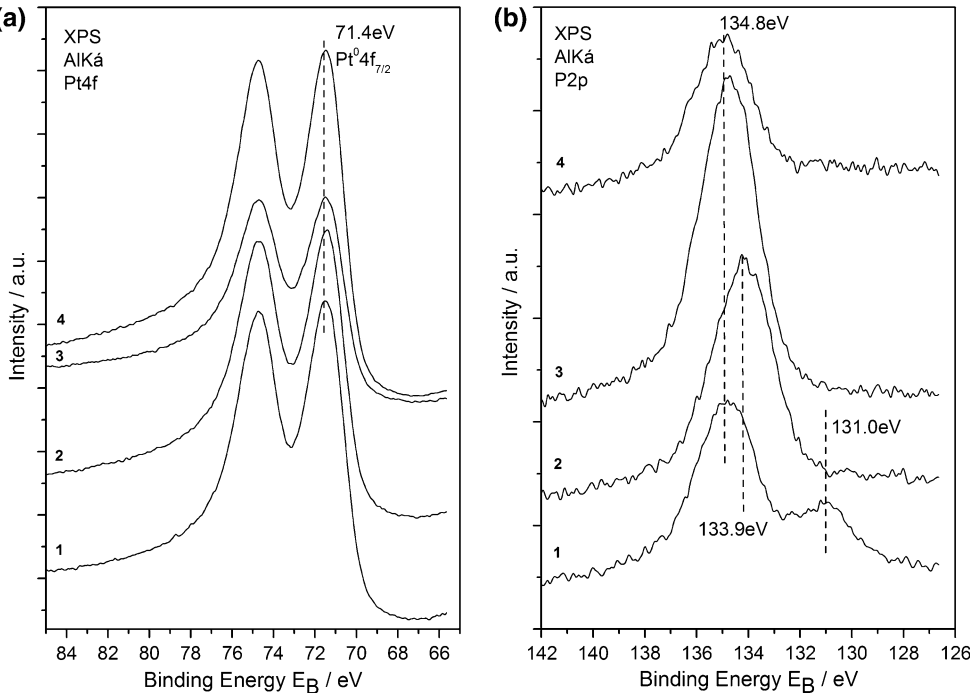

Fig. 11 XP spectra of Pt4f (**a**) and P2p (**b**), after heating at 200 °C for 4 h in H_2 flow (*1*), after heating at 180 °C for 1.5 h in 4 % H_2O/He flow (*2*), after heating at 200 °C for 4 h in UHV (*3*), and after heating at 200 °C for 4 h in CO flow (*4*)

[34]. Upon heating the sample to 200 °C for 4 h under vacuum, the P2p signal increases and shifts to higher binding energy positioned at 134.8 eV. This can be attributed to the dehydration of the ortho-phosphate species into pyrophosphates or even polyphosphates (pyro- or polyphosphoric acid). The P2p peak at 134.8 eV (spectra 1, 3, and 4), is assigned in the literature to pyrophosphoric acid or poly-phosphate species [35, 36]. After the exposure of the sample in humidified He at elevated temperature (180 °C), the ortho-phosphate peak at 133.9 eV is recovered. The increase in the signal corresponds to the increase in the P2p/Pt4f ratio (Fig. 13), thus showing a significant degree of restructuring of the PA/Pt film interface. This observation in combination to the observed decrease in CO oxidation peak in Fig. 10, after the long exposure of the electrode in dry Ar flow, strongly indicates that pyrophosphoric acid may block the Pt surface. Whereas in all other cases the decreased total P2p/Pt4f ratio indicates a displacement of the phosphoric or pyrophosphoric acid from the Pt surface by H_2, H_2O, and CO. It is worth noticing that long exposure of the sample under CO flow at elevated temperatures can even further displace pyrophosphoric acid as this is evidently shown in Fig. 13. The same trend was observed for the case of *O*/Pt ratio, showing that the measured O1s oxygen species are chemically combined in the various P and O containing adsorbed species.

Under dry H_2 flow for 4 h at 200 °C, a second peak appears at significantly lower binding energy (131 eV), which suggests the formation of a compound that originates from the catalytic reduction of the pyrophosphoric acid on the Pt surface. It is worth noticing that the species after H_2 treatment contain the smallest amount oxygen thus showing the severe reduction of the pyro/poly-phosphate species.

The data acquired from O1s peaks, give further insight confirming the previous conclusions. Figure 12 shows the XP Spectra of O1s peak. The peak is deconvoluted in all cases in two components with equal FWHM (Table 3). The binding energy difference is 1.5 eV. It has been reported that the O1s peak positions range between 531.6 and 532.6 eV (peak I) for non-bridging oxygen (NBO: PO^-,

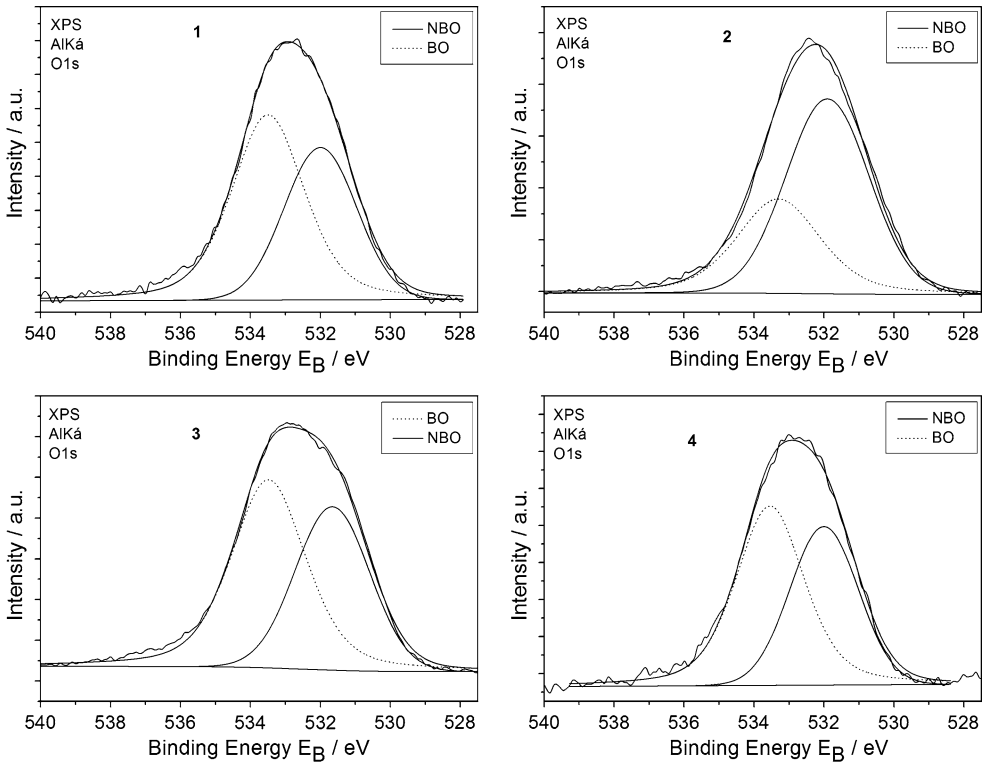

Fig. 12 XP spectra of O1s peaks after heating at 200 °C for 4 h in H_2 flow (*1*), at 180 °C for 1.5 h in 4 % H_2O/He flow (*2*), at 200 °C for 4 h in UHV (*3*), and at 200 °C for 4 h in CO flow (*4*)

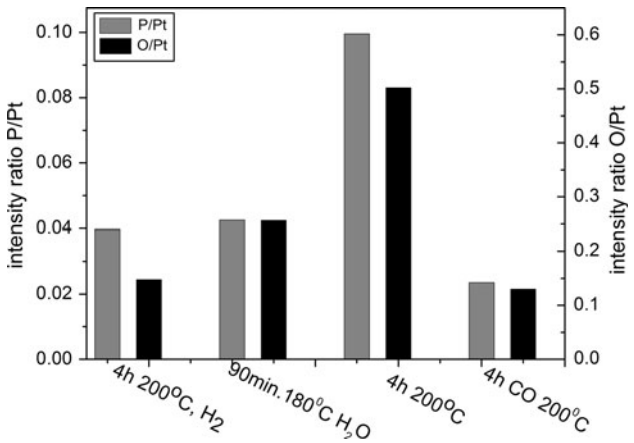

Fig. 13 Intensity ratio P2p/Pt4f and O1s/Pt4f after annealing at 200 °C for 4 h in H_2 flow, at 180 °C for 1.5 h in 4 % H_2O/He flow, at 200 °C for 4 h in UHV, and at 200 °C for 4 h in CO flow

POH, P=O), and 533.1 and 534.1 eV(peak II) for bridging oxygen (BO: P–O–P) [37]. The intensity ratio of these different chemical states is shown in Table 3 and can be considered as an indication of the most pronounced chemical structure of the various phosphoric acid species on the surface. It is deduced that increased peak intensity of the BO prompts to the formation of pyrophosphoric or polyphosphoric acid with bridging oxygen in their structure. Using the total peak area of Pt4f, O1s, and P2p peaks, in each experiment and the appropriate sensitivity factors (based on Wagner's collection and adjusted to the transmission characteristics of analyser EA10) and equations, the *O*/*P*, *O*/Pt, and *P*/Pt atomic ratio is determined (Table 3). As it is shown in Table 3, both the *O*/*P* and the peak II/peak I O1s ratios decrease after heating at 180 °C under vacuum, thus indicating the formation of pyrophosphates or polyphosphates. The *O*/*P* nominal atomic ratio for phosphoric acid or ortho-phosphates is 4, whereas for the case of pyrophosphoric acid or pyrophosphates is 3.5. Heating under H_2 atmosphere, the *O*/*P* ratio is even lower 2.48 (Table 3), thus implying further reduction of the phosphate or pyrophosphate species by abstraction of oxygen. The atomic ratio of O1s peak to P2p at 134.8 eV of spectrum 1 in Fig. 11 was found to be 3.3, which lies between the *O*/*P* ratios of spectra 2 and 3 in Fig. 11 and Table 3. According to the aforementioned considerations, P species appearing at P2p = 131 eV originates from the reduction of the pyrophosphate species containing significantly reduced oxygen amount. It must be noted that the peak at 131 eV cannot be attributed to elemental P^o as the latter appears according to the literature at 130 eV [38, 39]. Thus, it is proposed that the low binding energy peak originates from the catalytic reduction of pyro/poly-phosphate species by H_2 on the Pt surface through probably the abstraction of hydroxyl groups, thus leaving a phosphorous–oxygen polymeric structure which can account for the lower binding energy of the P2p. The hydroxyl removal may result into a lower oxygen content chemical structure,

thus resulting in the decrease of the valence of P and the increase of the electron density around the P atom. In this respect, we can possibly rationalize the significant decrease in binding energy by 3.5 eV.

3.4 The proposed mechanism

To summarize, after careful evaluation of all the above results, the following chemical mechanism can be responsible for Pt electrochemical active area loss, especially for the case of low PA amounts in the anodic catalyst layer (<3 gPA/gPt). During normal fuel cell operation, three processes occur at the anode electrode. The phosphoric acid is dehydrated, according to Eq. 5, into pyrophosphoric or polyphosphoric species which spreads and blocks the Pt surface.

$$\begin{aligned} 2H_3PO_4 &\rightarrow H_4P_2O_7 + H_2O \text{ or } nH_3PO_4 \\ &\rightarrow H_{n+2}P_nO_{3n+1} + n - 1\ H_2O. \end{aligned} \quad (5)$$

Displacement of phosphoric acid and the formed polyphosphoric species from the Pt surface is possible by H_2 adsorption and spill-over. Concurrently, polyphosphoric acid is being catalytically reduced most probably into an oxide form of P with less oxygen. The exact chemical structure of this oxidic species cannot be defined within the context of the present study. It is considered that this species covers and poisons the Pt surface. Upon exposure of the sample in humidified He ortho-phosphate species is recovered (Fig. 11, spectrum 2), thus showing the reversibility of the processes. The electrochemical oxidation of these species can take place during the CVs of Figs. 3, 4, 5, and 6 at 750 mV with the simultaneous recovery of the Pt surface. The electrochemical oxidation of reduced phosphoric acid species (hypophosphite $H2PO2^{-}$) on Ni surfaces has been reported in the literature [40].

It has been clearly shown that the PA amount sprayed on the anodic electrode influences the anode performance. At least for the studied high temperature MEA system, an inadequate amount of PA at the anodic electrode can lead to the gradual shrinking of the electrochemical interface, as well as a gradual "poisoning" of the Pt electrocatalyst by species originating from dehydrated and especially H_2 reduced chemical structures of PA.

Though one would expect that the poisoning effect of higher amount of PA on the anodic electrode would have been more severe, it turns out that the utilization of PA above a certain ratio (>3 gPA/gPt) to be beneficial, as the species that are oxidized at 750 mV or the shrinkage of the ECSA were not observed. This controversial behavior strongly indicates that this is directly related and limited to the catalytic interference of the PA with the Pt surface under lean hydration conditions, while the active water molecules can be provided through the absorbed water in the PA. It can be assumed that increased amount of distributed PA within the catalytic layer will absorb and store higher amount of water. In addition, the increased amount of PA and its fine distribution within the catalytic layer will result in a more extended Pt/PA interface, thus providing higher hydration degree onto the Pt surface. In this respect, the poisoning and blocking species can be displaced from the Pt surface. Another significant reason for the beneficial role of the increased PA amount in the catalytic layer is to compensate its displacement either by H_2 or CO as this is clearly shown in Fig. 13b, thus providing the necessary boundary length of the electrochemical interface to facilitate the H_2 electrooxidation. As was formerly stated [41], the amount/concentration of water plays an autocatalytic role for the facilitation of H_2 electrochemical oxidation on PA imbibed high temperature PEM electrochemical interface.

4 Conclusions

It was observed that the reversible performance loss of the anodic electrode was a function of the PA amount in the catalyst layer. More specifically, under low PA loading (<3 gPA/gPt) on the anodic electrode, <10 % of the Pt active surface is electrochemically active under fuel cell operating conditions. This was attributed to the blockage of the Pt surface by pyrophosphoric acid or polyphosphates, H_2 reduced polyphosphoric acid species and the shrinkage of the interface due to the displacement of the H_3PO_4 by the adsorbed H_2 species. The results are dramatically different for high PA loadings, where it was found that the Pt surface utilization was very high (>80 %) and has been attributed to the enhanced degree of the hydration of the electrochemical interface that accompanies the more uniform distribution of the H_3PO_4 within the catalytic layer. The controlled and increased PA content within the catalytic layer can result even up to the tenfold decrease in the Pt loading when the anode operates under H_2-rich conditions.

Acknowledgments Financial support of this work from the European Commission through the program "Understanding the Degradation Mechanisms of Membrane-Electrode-Assembly for High Temperature PEMFCs and Optimization of the Individual Components," DEMMEA FCH-JU 245156 (2010–2012) is greatly acknowledged.

References

1. Yang C, Costamagna P, Srinivasan S, Benziger J, Bocarsly AB (2001) Approaches and technical challenges to high temperature operation of proton exchange membrane fuel cells. J Power Sources 103(1):1–9. doi:10.1016/S0378-7753(01)00812-6

2. Song JM, Suzuki S, Uchida H, Watanabe M (2006) Preparation of high catalyst utilization electrodes for polymer electrolyte fuel cells. Langmuir 22(14):6422–6428. doi:10.1021/la060671w
3. Xu Z, Qi Z, Kaufman A (2005) Superior catalysts for proton exchange membrane fuel cells. Electrochem Solid State Lett 8(6):A313–A315. doi:10.1149/1.1912018
4. Kim H, Lee W, Yoo D (2007) Functionalized carbon support with sulfonated polymer for direct methanol fuel cells. Electrochim Acta 52(7):2620–2624. doi:10.1016/j.electacta.2006.09.017
5. Du CY, Zhao TS, Liang ZX (2008) Sulfonation of carbon-nanotube supported platinum catalysts for polymer electrolyte fuel cells. J Power Sources 176(1):9–15. doi:10.1016/j.jpowsour.2007.10.016
6. Orfanidi A, Daletou MK, Neophytides SG (2011) Preparation and characterization of Pt on modified multi-wall carbon nanotubes to be used as electrocatalysts for high temperature fuel cell applications. Appl Catal B Environ 106:379–389. doi:10.1016/j.apcatb.2011.05.043
7. Pefkianakis EK, Deimede V, Daletou MK, Gourdoupi N, Kallitsis JK (2005) Novel polymer electrolyte membrane, based on pyridine containing poly(ether sulfone), for application in high-temperature fuel cells. Macromol Rapid Commun 26:1724–1728. doi:10.1002/marc.200500540
8. Daletou MK, Geormezi M, Pefkianakis EK, Morfopoulou C, Kallitsis JK (2010) Fully aromatic copolyethers for high temperature polymer electrolyte membrane fuel cells. Fuel Cells 10(1):35–44. doi:10.1002/fuce.200900032
9. Kalamaras I, Daletou MK, Gregoriou VG, Kallitsis JK (2011) Sulfonated aromatic polyethers containing pyridine units as electrolytes for high temperature fuel cells. Fuel Cells 11:921–931. doi:10.1002/fuce.201100024
10. Geormezi M, Chochos CL, Gourdoupi N, Neophytides SG, Kallitsis JK (2011) High performance polymer electrolytes based on main and side chain pyridine aromatic polyethers for high and medium temperature proton exchange membrane fuel cells. J Power Sources 196:9382–9390. doi:10.1016/j.jpowsour.2011.06.031
11. Kalamaras I, Daletou MK, Neophytides SG, Kallitsis JK (2012) Thermal crosslinking of aromatic polyethers bearing pyridine groups for use as high temperature polymer electrolytes. J Membr Sci 415–416:42–50. doi:10.1016/j.memsci.2012.04.057
12. Li Q, Jensen JO, Savinell RF, Bjerrum NJ (2009) High temperature proton exchange membranes based on polybenzimidazoles for fuel cells. Prog Polym Sci 34(5):449–477. doi:10.1016/j.progpolymsci.2008.12.003
13. Daletou MK, Kallitsis JK, Voyiatzis G, Neophytides SG (2009) The interaction of water vapors with H_3PO_4 imbibed electrolyte based on PBI/polysulfone copolymer blends. J Membr Sci 326:76–83. doi:10.1016/j.memsci.2008.09.040
14. Norskov JK, Rossmeisl J, Logadottir A, Lindqvist L, Kitchin JR, Bligaard T, Jonsson H (2004) J Phys Chem B 108:17886–17892. doi:10.1021/jp047349j
15. Nart FC, Iwasita T (1992) On the adsorption of $H_2PO_4^-$ and H_3PO_4 on platinum: an in situ FT-*ir* study. Electrochim Acta 37(3):385–391. doi:10.1016/0013-4686(92)87026-V
16. Habib MA, Bockris JO'M (1985) Adsorption at the solid/solution interface, an FTIR study of phosphoric acid on platinum and gold. J Electrochem Soc 132(1):108–114. doi:10.1149/1.2113736
17. Das SK, Reis A, Berry KJ (2009) Experimental evaluation of CO poisoning on the performance of a high temperature proton exchange membrane fuel cell. J Power Sources 193:691–698. doi:10.1016/j.jpowsour.2009.04.021
18. Camargo APM, Previdello BAF, Varela H, Gonzalez ER (2010) Effect of temperature on the electro-oxidation of ethanol on platinum. Quim Nova 33:2143–2147. doi:10.1590/S0100-40422010001000026
19. Kohlmayr G, Stonehart P (1973) Adsorption kinetics for carbon monoxide on platinum in hot phosphoric acid. J Electrochim Acta 18(2):211–223. doi:10.1016/0013-4686(73)80014-3
20. Bagotzky VS, Vassilyev YuB, Weber J, Pirtskhalava JN (1970) Adsorption of anions on smooth platinum electrodes. J Electroanal Chem Interfacial Electrochem 27(1):31–46. doi:10.1016/S0022-0728(70)80200-5
21. Vidaković T, Christov M, Sundmacher K (2007) The use of CO stripping for in situ fuel cell catalyst characterization. Electrochim Acta 52:5606–5613. doi:10.1016/j.electacta.2006.12.057
22. Jiang R, Russell Kunz H, Fenton JM (2006) Influence of temperature and relative humidity on performance and CO tolerance of PEM fuel cells with Nafion®–Teflon®–$Zr(HPO_4)_2$ higher temperature composite membranes. Electrochim Acta 51(26):5596–5605. doi:10.1016/j.electacta.2006.02.033
23. Buelte SJ, Lewis D, Eisman G (2011) Effects of phosphoric acid concentration on platinum catalyst and phosphoric acid hydrogen pump performance. ECS Trans 41(1):1955–1966. doi:10.1149/1.3635725
24. Vogel WM, Baris JM (1978) Changes in the surface of platinum in hot concentrated phosphoric acid at low potentials. J Electrochim Acta 23:463–466. doi:10.1016/0013-4686(78)87047-9
25. Sugishima N, Hinatsu JT, Foulkes FR (1994) Phosphorous acid impurities in phosphoric acid fuel cell electrolytes II. Effects on the oxygen reduction reaction at platinum electrodes. J Electrochem Soc 141:3332–3335. doi:10.1149/1.2059335
26. Huang JC, Sen RK, Yeager E (1979) Oxygen reduction on platinum in 85 % orthophosphoric acid. J Electrochem Soc 126:786–792. doi:10.1149/1.2129139
27. Clouser SJ, Huang JC, Yeager E (1993) Temperature dependence of the Tafel slope for oxygen reduction on platinum in concentrated phosphoric acid. J Appl Electrochem 23:597–605. doi:10.1007/BF00721951
28. Sugishima N, Hinatsu JT, Foulkes FR (1994) Phosphorous acid impurities in phosphoric acid fuel cell electrolytes I. Voltammetric study of impurity formation. J Electrochem Soc 141:3325–3331. doi:10.1149/1.2059334
29. Camargo APM, Previdello BAF, Varela H, Gonzalez ER (2010) The impact of water concentration on the catalytic oxidation of ethanol on platinum electrode in concentrated phosphoric acid. Electrochem Commun 12:140–143. doi:10.1016/j.elecom.2009.11.008
30. Burke LD, Morrissey JA (1994) Hydrous oxide formation on platinum in phosphoric acid solution. J Electrochem Soc 141:2361–2368. doi:10.1149/1.2055126
31. Burke LD, Casey JK (1992) The role of hydrous oxide species on platinum electrocatalysts in the methanol/air fuel cell. Electrochim Acta 37:1817–1829. doi:10.1016/0013-4686(92)85086-Z
32. Sleightholme AES, Kucernak A (2011) An anomalous peak observed in the electrochemistry of the platinum/perfluorosulfonic acid membrane interface. Electrochim Acta 56:4396–4402. doi:10.1016/j.electacta.2010.12.036
33. Parkinson CR, Walker M, McConville CF (2003) Reaction of atomic oxygen with a Pt(111) surface: chemical and structural determination using XPS, CAICISS and LEED. Surf Sci 545:19–33. doi:10.1016/j.susc.2003.08.029
34. Heuberger R, Rossi A, Spencer ND (2006) XPS study of the influence of temperature on ZnDTP tribofilm composition. Tribol Lett 25(3):185–196. doi:10.1007/s11249-006-9166-9
35. Deng J, Wang J, Xu X, Huang H-H, Xu G-Q (1996) Oxidative dehydrogenation of glycol to glyoxal on a P-modified electrolytic silver catalyst. Catal Lett 36(3–4):207–214
36. Zhou JG, Thompson J, Cutler J, Blyth R, Kasrai M, Bancroft GM, Yamaguchi E (2010) Resolving the chemical variation of phosphates in thin ZDDP tribofilms by X-ray photoelectron spectroscopy using synchrotron radiation: evidence for ultraphosphates and

organic phosphates. Tribol Lett 39(1):101–107. doi:10.1007/s11249-010-9619-z
37. Eglin M, Rossi A, Spencer ND (2003) X-ray photoelectron spectroscopy analysis of tribostressed samples in the presence of ZnDTP: a combinatorial approach. Tribol Lett 15(3):199–209. doi:1023-8883/03/1000-0199/0
38. Thøgersen A, Syre M, Olaisen BR, Diplas S (2013) Studies of the oxidation states of phosphorus gettered silicon substrates using X-ray photoelectron spectroscopy and transmission electron microscopy. J Appl Phys 113:044307. doi:10.1063/1.4775818
39. Li H, Wang W, Chen H, Deng J (2001) Surface morphology and electronic state characterization of Ni–P amorphous alloy films. J Non Cryst Solids 281(1–3):31–38. doi:10.1016/S0022-3093(00)00430-0
40. Zeng Y, Zhou S (1999) In situ UV–Vis spectroscopic study of the electrocatalytic oxidation of hypophosphite on a nickel electrode. Electrochem Commun 1(6):217–222. doi:10.1016/S1388-2481(99)00043-0
41. Daletou MK, Kallitsis JK, Neophytides SG (2011) Materials, proton conductivity and electrocatalysis in high temperature PEM fuel cells. In: Vayenas SC (ed) Interfacial phenomena in electrochemistry, modern aspects of electrochemistry, vol 51. Springer, New York, pp 301–368. doi:10.1007/978-1-4419-5580-7_6